

Dissecting the Lyman α emission halo of LAB1

Anne-Marie Weijmans^{1,2*}, Richard G. Bower³, James E. Geach³,
A. Mark Swinbank³, R. J. Wilman⁴, P. T. de Zeeuw^{5,1} and Simon L. Morris³

¹ *Sterrewacht Leiden, Leiden University, Postbus 9513, 2300 RA Leiden, The Netherlands*

² *Dunlap Institute for Astronomy & Astrophysics, University of Toronto, 50 St. George Street, Toronto, ON M5S 3H4, Canada*

³ *Institute for Computational Cosmology, Department of Physics, Durham University, South Road, Durham, DH1 3LE, UK*

⁴ *Centre for Astrophysics & Supercomputing, Swinburne University of Technology, Hawthorn, Victoria 3122, Australia*

⁵ *European Southern Observatory, Karl-Schwarzschild-Str 2, 85748 Garching, Germany*

17 June 2018

ABSTRACT

We report observations of Lyman Alpha Blob 1 (LAB1) in the SSA 22 protocluster region ($z = 3.09$) with the integral-field spectrograph SAURON. We increased the signal-to-noise in the spectra by more than a factor three compared to our previous observations. This allows us to probe the structure of the LAB system in detail, examining its structure in the spatial and wavelength dimensions. We find that the emission from the system comes largely from five distinct blobs. Two of the emission regions are associated with Lyman Break Galaxies, while a third appears to be associated with a heavily obscured submillimeter galaxy. The fourth and fifth components do not appear to be associated with any galaxy despite the deep imaging that is available in this field. If we interpret wavelength shifts in the line centroid as velocity structure in the underlying gas, many of these emission systems show evidence of velocity shear. It remains difficult to distinguish between an underlying rotation of the gas and an outflow driven by the central object. We have examined all of the line profiles for evidence of strong absorption features. While several systems are better fitted by the inclusion of a weak absorption component, we do not see evidence for a large-scale coherent absorption feature such as that seen in LAB2.

Key words: galaxies: haloes — galaxies: high redshift

1 INTRODUCTION

By allowing us to probe the gaseous haloes around $z \sim 3$ galaxies, large scale Lyman α nebulae provide a fascinating insight into the formation of high-redshift galaxies. The first and brightest of these haloes were discovered by Steidel et al. (2000) in the SSA 22 protocluster region at $z = 3.09$. Subsequently a population of fainter Lyman Alpha Blobs (LABs) was detected in deep narrow-band imaging surveys (e.g. Matsuda et al. 2004; Nilsson et al. 2006; Smith & Jarvis 2007), revealing that LABs have a large spread in properties such as surface brightness and morphology, and it has been suggested that their presence is linked to dense environments (Matsuda et al. 2004). Follow-up observations in the optical, near-infrared and particularly the far-infrared suggest that LABs are sites of massive galaxy formation, enhanced by the cluster environment (e.g. Chapman et al. 2004). This view is supported by the discovery of luminous submillime-

ter sources in several LABs (e.g. Geach et al. 2005). LAB systems like those discovered by Steidel et al. (2000) are also found around high-redshift radio galaxies (e.g. Chambers, Miley & van Breugel 1990; Villar-Martín et al. 2002). However, the study of such radio loud systems is complicated by the presence of radio jets and lobes. It is unclear whether these systems are directly comparable to the radio quiet LABs that we discuss in this paper, or that they have a different power source, such as the injection of cosmic rays by the radio source (e.g. Ferland et al. 2009).

The origin of radio quiet LABs is still unclear, and three different scenarios have been proposed to explain their existence. One is that the gas in LABs is heated by photo-ionisation, caused by massive stars and/or active galactic nuclei (AGN) (Geach et al. 2009). However, for one third of the LABs in the sample of Matsuda et al. (2004), the observed UV luminosities are too low to produce the observed Ly α radiation, although putative ionising sources could be obscured along our line of sight. For example, Geach et al. (2009) argue that in a large fraction of LABs there is suffi-

* E-mail: weijmans@di.utoronto.ca

cient UV flux from an obscured AGN component to power the extended line emission, despite large dust covering fractions. While photo-ionisation is likely to play a role in powering LABs, it is nonetheless instructive to consider alternative or additional power sources for the Ly α emission in LABs, since it is not clear that a single mechanism (such as photo-ionisation) is responsible for all of the observed properties of these objects.

An alternative scenario is that the gas in LABs is excited by cooling flows (e.g. Haiman, Spaans & Quataert 2000; Fardal et al. 2001; Dijkstra & Loeb 2009). Nilsson et al. (2006) argue that the emission in the LAB they detected in the GOODS South field originates from cold accretion onto a dark matter halo. This view is supported by the lack of continuum counterparts, which could photo-ionise the gas, and the absence of a massive starburst in the infrared, that could point to a superwind outflow (see below). Instead, they find a good match between their observed surface brightness profile and the profiles derived from theoretical models for collapsing clouds from Dijkstra, Haiman & Spaans (2006). A similar analysis is given by Smith et al. (2008) for the LAB presented in Smith & Jarvis (2007).

The third proposed origin for extended Ly α emission haloes is provided by the so-called superwind model (e.g. Taniguchi & Shioya 2000; Ohyama et al. 2003). After an initial starburst, massive stars die in supernovae. If the resulting supernova remnants overlap, they could form a super-bubble (e.g. Heckman, Armus & Miley 1990), from which a superwind can blow gas into the intergalactic medium if the kinetic energy in the gas is large enough to overcome the gravitational potential. Taniguchi & Ohyama (2000) suggest an evolutionary sequence for elliptical galaxies that includes LABs. During the initial starburst, a galaxy can be enshrouded by gas and dust grains, and is therefore observable as a (dusty) submillimeter source. The LABs represent the subsequent superwind phase, expelling the gas and dust, and therefore rendering the galaxy fainter in the submillimeter regime. After this phase, the galaxy continues to develop into a normal elliptical galaxy.

The brightest and most extended LAB observed to date is LAB1 (SSA22a-C11), one of the two LABs described by Steidel et al. (2000). This LAB has a Ly α luminosity of 1.1×10^{44} ergs s $^{-1}$ at $z = 3.1$ (Matsuda et al. 2004), and a spatial extent of ~ 100 kpc. Matsuda et al. (2004) find bubble-like structures in narrowband images of LAB1, in support of the superwind model for this LAB. Bower et al. (2004) observed LAB1 with the integral-field spectrograph SAURON (Bacon et al. 2001). They found extensive emission, and a large velocity dispersion for the Ly α emission line (~ 500 km s $^{-1}$). Although interpretation of the spectra of LAB1 is not straightforward, since Ly α is a resonant line and therefore emission can easily get scattered, they find similarities between LAB1 and the local emission-line halo of NGC 1275 in the Perseus cluster. Longer observations of LAB2 with the same spectrograph suggested the existence of a dense outflowing shell of material around this system (Wilman et al. 2005). However, spectra of higher signal-to-noise are needed to find evidence for outflows in LAB1.

We therefore reobserved LAB1 with SAURON, adding signal to the data already published by Bower et al. (2004). By increasing the observing time from 9 hours in the original dataset to 23.5 hours in our new datacube, we increased the

signal-to-noise in the spectra, and therefore were able to obtain line profiles and kinematic maps of the Ly α emission in this region. We describe the new observations and data reduction of LAB1 in Section 2 and analyse the spectra in Section 3. In Section 4 we discuss our results and speculate on the structure and origin of LAB1. Throughout this paper, we assume a flat cosmology with $H_0 = 70$ km s $^{-1}$ Mpc $^{-1}$, $\Omega = 0.3$ and $\Lambda = 0.7$. In this scenario, 1 arcsec at $z = 3.1$ corresponds to 7.5 kpc.

2 OBSERVATIONS AND DATA REDUCTION

LAB1 was previously observed for 9 hours with SAURON at the William Herschel Telescope at La Palma, Spain, in July 2002. The relatively large field-of-view (41×33 arcsec 2) and high throughput (20 per cent) make this spectrograph a very suitable instrument for deep Ly α observations, even though it was originally built to study the dynamics and stellar populations of nearby early-type galaxies (de Zeeuw et al. 2002). The relatively high spectral resolution of 4.2 Å (FWHM) of the instrument, in combination with the wide field, was obtained by compromising on the total wavelength coverage (4810 to 5350 Å). As a result, SAURON can observe Ly α systems at redshifts $2.96 < z < 3.40$, and fortunately, LAB1 resides within this redshift range ($z = 3.1$). A description of the earlier observations of LAB1 and their reduction can be found in Bower et al. (2004).

In these previous observations, we lacked the signal-to-noise (S/N) to search for asymmetries in the line profiles and signs for possible neutral absorption, as found in SAURON spectra of LAB2 by Wilman et al. (2005). We therefore reobserved LAB1 for an additional 15 hours with SAURON, between 15 and 21 September 2006. The observations were split into individual exposures of 1800 seconds and dithered by a few arcseconds. The data were reduced using the dedicated XSAURON software (Bacon et al. 2001). We replaced our calibration frames, to correct for a malfunctioning shutter (see Weijmans et al. 2009 for more details). We had also observed six blank sky fields, and created a so-called superflat by taking the smoothed median of these blank frames and the dithered object frames in the spectral direction. Dividing our already flat-fielded data by this superflat removed most of the remaining flat-field residuals. The spectra were degraded to a resolution of 4.9 Å (FWHM) to be consistent with the LAB1 observations of Bower et al. (2004), and sky subtracted with the signal from the SAURON skylenslets, that obtain simultaneous sky spectra pointing 2 arcminutes away from the main field-of-view.

Before merging this new dataset with the cubes of Bower et al. (2004), we first re-reduced these spectra in the same way as described above to make sure that both datasets were treated identically. One of the frames had to be discarded because of bad sky subtraction. The remaining 17 frames of the old dataset were then merged with the 30 frames of the new dataset, using a faint star in the south-east corner of the field-of-view to align the cubes. In the merged cube, this star has a FWHM of 1.3 arcsec. We set the spatial resolution of the cube to 0.4 arcsec per pixel, while the spectral resolution is 1.15 Å per pixel. This final cube represents 23.5 hours of observing time, and is the deepest SAURON observation to date. The increase in S/N

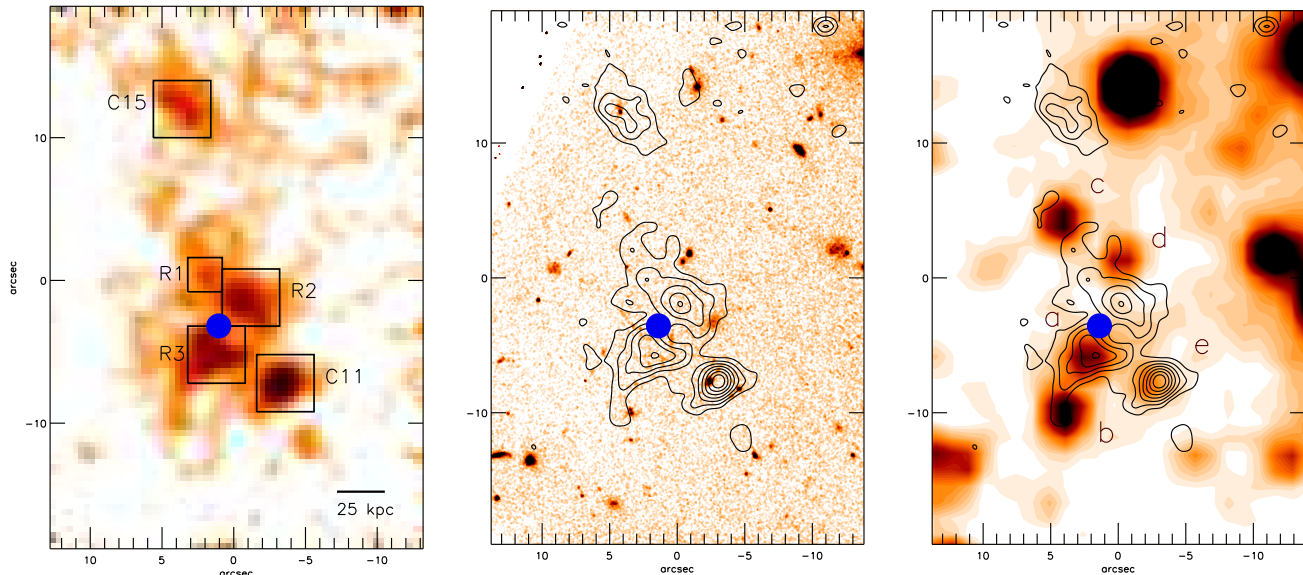


Figure 1. Ly α emission in the LAB1 region. Left panel: continuum subtracted Ly α emission, obtained from collapsing the SAURON spectra over a narrow wavelength range centred on the emission line. Interesting regions are indicated by boxes (see text). Middle panel: *HST*/STIS optical image overlaid with Ly α contours from the left panel. The faintest contour has a surface brightness of 5.6×10^{-18} erg s $^{-1}$ cm $^{-2}$ arcsec $^{-2}$ and contours increase in steps of 3.7×10^{-18} erg s $^{-1}$ cm $^{-2}$ arcsec $^{-2}$. Note however the 50 per cent uncertainty in absolute flux calibration (see §2). Right panel: same as middle panel, but now a *Spitzer*/IRAC 3.6 μ m image is displayed. Sources identified in Geach et al. (2007) are indicated with identical nomenclature (*a-e*). In all plots, the blue dot denotes the position of the radio source (Chapman et al. 2004). All images are plotted on the same scale and are orientated such that North is up and East to the left.

is a factor of 3.7 compared to the dataset of Bower et al. (2004), which is more than would be expected based on the factor 2.6 increase in exposure time. The higher than expected *S/N* results from improved observing and data reduction techniques, developed over the past few years within the SAURON team.

Unfortunately, due to the malfunctioning shutter of the spectrograph we could not observe flux stars during the 2006 observing run. However, since relative run-to-run variations in spectral response of SAURON have been shown to be smaller than 1 per cent (Kuntschner et al. 2006), we could still perform a relative flux calibration using flux star observations from a previous run. An absolute flux calibration of our data was done using flux values for C15 from the literature. We added the flux in a wavelength interval centred around the Ly α line ($4960 \text{ \AA} < \lambda < 5000 \text{ \AA}$) in a 4×4 arcsec 2 box around C15, and scaled the number of counts to the flux given by Matsuda et al. (2004). We checked our conversion factor with Bower et al. (2004), and found a deviation of 50 per cent. As the flux calibration is the main source of uncertainty, we adopt this deviation to estimate the errors on our obtained fluxes (see Table 1).

3 ANALYSIS

3.1 The halo structure of LAB1

In Figure 1 we show a continuum subtracted Ly α image of LAB1, obtained by integrating the spectra in our SAURON datacube over a small wavelength range (4960 - 5040 \AA)

containing the redshifted emission line. The most striking result is that LAB1 is not one coherent structure, but that the emission is concentrated in five distinct emission regions (labeled R1-R3, C11, C15), embedded in a Ly α emission halo (see also Matsuda et al. 2004). These five regions were selected primarily by eye, exceeding the third contour level in Figure 1, corresponding to 1.3×10^{-17} erg s $^{-1}$ cm $^{-2}$ arcsec $^{-2}$. We estimate that about 55 per cent of the total Ly α emission can be associated with one of these regions. Thus it appears that the giant emission halo results from a combination of smaller emission blobs, comparable to the more typical LABs identified by Matsuda et al. (2004).

In order to attempt to identify each of the Ly α blobs (R1-R3, C11 and C15) with underlying galaxies, we overlay the Ly α emission line contours of our cube with an *HST*/STIS image and a *Spitzer*/IRAC 3.6 μ m image (see Figure 1). Geach et al. (2007) used the same images as well as MIPS 24 μ m imaging to identify IRAC counterparts in the LAB1 region. They found five sources, labeled *a-e* in Figure 1, of which two (*c* and *d*) have mid-infrared colours inconsistent with galaxies at $z = 3.1$, and therefore are most likely not part of the proto-cluster. The IRAC source *b* is located at the southern extreme of LAB1, and the new SAURON observations reveal that it is not coincident with a peak in the Ly α emission (although there is some low-surface brightness emission extending from the north). The two remaining IRAC sources, *a* and *e*, seem to be related to the Ly α emission. We discuss the Ly α emission blobs in more detail below.

Two of the brightest Ly α emitting regions (C11 and

C15) were identified with Lyman Break Galaxies (LBGs) by Steidel et al. (2000). These can be clearly seen in the STIS continuum image. The positional uncertainty between the Ly α emission and continuum detection in the STIS image is less than 1.5 arcsec. C11 is also weakly detected in the IRAC bands (source *e*), with a 3.6 μm flux of 1.5 μJy . C15 was labeled by Matsuda et al. (2004) as LAB8, as this blob is clearly separated from the main emission halo. Neither C15 nor C11 is detected in X-ray ($L_X < 2.0 \times 10^{43}$ ergs s^{-1} , 2-43 keV band) in the deep *Chandra* exposures of this region (Geach et al. 2009).

The bright Ly α blob R3 is associated with an extremely red galaxy (source *a* in Geach et al. 2007) and thought to be the counterpart to a bright submillimeter source detected by Chapman et al. (2001; 2004). This source has an unresolved submillimeter flux of $S_{850\mu\text{m}} = 16.8 \pm 2.9$ mJy and $S_{450\mu\text{m}} = 45.1 \pm 15.5$ mJy, measured with the Submillimeter Common-User Bolometer Array (SCUBA). The peak of the Ly α emission of R3 lies within 1.3 arcsec of the submillimeter centroid, and 0.7 arcsec of the IRAC counterpart *a*. Higher resolution submillimeter observations with the Submillimeter Array (SMA) (Matsuda et al. 2007) yielded no detection, and hinted that the submillimeter emission could originate from an extended starburst component on scales of >4 arcseconds (>30 kpc), and indeed this source is coincident with several low-surface brightness UV components in the STIS imaging.

Nearby tentative radio and CO detections (Chapman et al. 2004) further re-inforce the view that the submillimeter source is associated with the IRAC source *a*, and therefore most likely with Ly α blob R3. Because of the large positional uncertainties on the radio detection, which could be consistent with either the submillimeter source or the cavity in the Ly α emission that separates R3 from R2, we prefer to associate the radio source with the submillimeter source, given the strong association between those identifications in other submillimeter studies (e.g. Ivison et al. 2007). Assuming a modified blackbody spectrum with characteristic temperature $T_d = 35$ K (Blain, Barnard & Chapman 2003), the observed 850 μm flux corresponds to a bolometric luminosity of $L_{\text{bol}} = 1.5 \times 10^{13} L_{\odot}$. If this luminosity arises from starformation alone with a standard IMF (Kennicutt 1998), then the implied star formation rate (SFR) is $\sim 2500 M_{\odot} \text{yr}^{-1}$. We note that an AGN contribution in LAB1 is not likely to significantly affect this result: LAB1 is not detected in a 400 ks *Chandra* exposure, with a luminosity limit $L_X < 2.4 \times 10^{43}$ ergs s^{-1} in the 2–32 keV band (Geach et al. 2009). The most likely scenario is that source *a* is dominated by a dusty, potentially extended, starburst.

In contrast to C11, C15 and R3, the Ly α emission regions R1 and R2 do not appear to have either an optical or a mid-infra red counterpart (down to a 3.6 μm flux of $< 1\mu\text{Jy}$). Given the depth of the IRAC imaging of this field it seems unlikely that these sources are identified with a dust obscured galaxy. Although offsets of several arcseconds are also seen in the field Ly α emission survey of Matsuda et al. (2004), analysis of the optical to mid-IR colours suggests that the nearest IRAC source *d* is not part of the proto-cluster system. An appealing possibility is therefore that components R1 and R2 are genuinely associated with gas trapped, and possibly cooling, within the proto-cluster potential. R1 and R2 are at the same velocity as the other

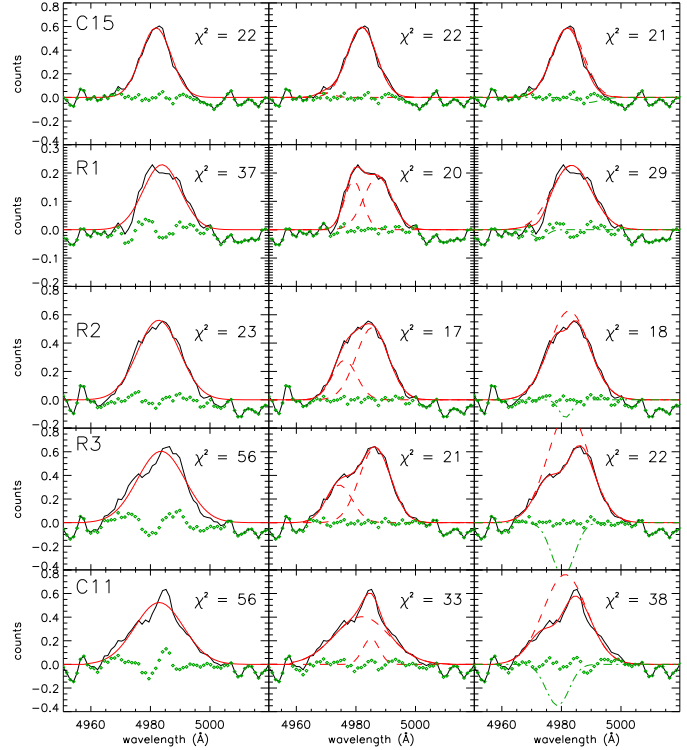


Figure 2. Single Gaussian (left), double Gaussian (middle) and combined Gaussian emission and Voigt absorption profiles (right) fitted to the spectra in indicated regions of Figure 1. Rows show the spectra and fits for different blobs, as indicated in the upper left corner of the left panel. The observed spectra are shown in black, while the fit is overplotted in red. Dashed red lines show Gaussian profiles, and in the right hand panels the green dotted-dashed line indicates the absorber. The green dots show the residuals of the fit. All fits have been convolved with the instrumental dispersion profile of 108 km s^{-1} . See Table 2 for the fitted parameters.

components in LAB1 and show no clear signs of outflow (see §3.3) or association with continuum sources. This highlights the diverse range of physics that could be contributing to the overall Ly α emission structure, which is perhaps powered by a combination of feedback from young active galaxies and energy released from the cooling of pristine gas.

3.2 Emission line profiles

One of the principle goals of our deeper observations was to analyse the structure of LAB1 as a function of wavelength in search of outflows and coherent absorption line systems, such as seen in LAB2 (Wilman et al. 2005). To analyse the line profiles, we bin the spectra of each blob in a square region centred on the emission peak. Each square has sides of 4 arcsec to enclose the separate blobs, except for the smaller blob R1, where we used a square with sides of 2.4 arcsec (Figure 1). We initially fit the resulting spectra with a single Gaussian emission line, but with the exception of C15 and R2 this provides a poor fit to the data. Better fits are obtained by instead modeling the line shape with a double Gaussian or a Gaussian emission profile combined with a Voigt absorption profile (for details of the fitting procedure see Wilman et al. 2005). In the case of absorption, the wave-

Field	α	δ	L (Ly α) erg s $^{-1}$	STIS mag	$m_{3.6\mu\text{m}}$ mag
C15	22 ^h 17 ^m 26.1 ^s	00 $^{\circ}$ 12' 54.1''	1.7×10^{43}	26.13 ± 0.02	>23.7
R1	22 ^h 17 ^m 26.0 ^s	00 $^{\circ}$ 12' 42.5''	8.4×10^{42}	>27.42	>23.7
R2	22 ^h 17 ^m 25.8 ^s	00 $^{\circ}$ 12' 40.9''	2.3×10^{43}	>27.42	>23.7
R3	22 ^h 17 ^m 26.0 ^s	00 $^{\circ}$ 12' 36.9''	2.7×10^{43}	>27.42	22.6 ± 0.1
C11	22 ^h 17 ^m 25.6 ^s	00 $^{\circ}$ 12' 34.9''	2.3×10^{43}	24.21 ± 0.01	23.6 ± 0.1

Table 1. Ly α blobs indicated in Figure 1. Coordinates are provided in J2000 notation. The uncertainties in the observed Ly α luminosity are around 50 per cent (see §2). The last two columns give the optical (*HST*/STIS) and infrared (*Spitzer*/IRAC 3.6 μm) fluxes in AB magnitudes. The IRAC fluxes have been measured in circular apertures of 4 arcsec diameter, and corrected for a small aperture loss. Lower magnitude limits for non-detections are 3σ limits.

length of the underlying Gaussian profile and Voigt profile are allowed to vary freely, but we found that if we allowed both the column density and equivalent width of the absorption to vary, the solutions were too degenerate because of their position on the curve of growth. We therefore fixed the column density at $3 \times 10^{14} \text{ cm}^{-2}$, typical of the range of the fits when this parameter was left free.

As Figure 2 shows, a clear improvement (a change in χ^2 larger than 3σ) for R1, R3 and C11 is obtained by including the absorber, or by allowing multiple Gaussian components. For R2, the fit improves, but the improvement in χ^2 is not significant. These fits cannot, however, discern between a situation with multiple emission sources or an absorbing medium. Moreover, the double Gaussian fits can be a mere reflection of the underlying velocity field of each source, as we sum spectra over relatively large apertures. We will explore this in more detail in §3.3.

In Table 2 we show the parameters of the best fits. It is remarkable that the redshift of the underlying Gaussian emission lines between the various components is $z = 3.099 \pm 0.001$ and varies in the restframe by less than 150 km s^{-1} over the whole region. This supports the interpretation of the LAB1 system as a high-redshift virialised group. The Gaussian line-widths are $\sigma \sim 400 \text{ km s}^{-1}$, measured in the restframe of the cluster, which is a typical value for LABs. In contrast to the case in LAB2 (Wilman et al. 2005) we do not find that the absorption is particularly strong, nor is the redshift of the absorber constant across the system. In LAB2 we used this to argue for the existence of a large-scale absorbing shell of outflowing material. In LAB1 we find no evidence for such a feature: indeed the strength of these putative absorption systems is such that they might well arise in the Lyman-alpha forest surrounding the LAB1 system (Wilman et al. 2004). Rest-frame UV spectroscopy of C11 presented by Shapley et al. (2006) suggests velocity offsets of 380 km s^{-1} between the Ly α emission and the ISM. This is larger, but quantitatively similar to the offset of 220 km s^{-1} that we derive between the peak of the Ly α emitter and the blue-shifted absorber, thus suggesting that the absorber seen in our Ly α profile is likely associated with the same ISM inferred from Shapley et al. (2006) (i.e. at the same redshift of the galaxy).

3.3 Kinematic signatures of outflow or rotation

Given that the line profiles are generally better matched by a more complex profile, we investigated the three-dimensional

structure of the emission in each of the emission regions. Since we find no strong evidence for absorption, it is likely that the line profiles arise from velocity shear in the emission surrounding each of the systems. In the discussion that follows we will implicitly assume that the shift occurs as a response to the bulk velocity of the emitting gas. The reader should be aware, however, that the line profile has a complex interaction with the gas velocity field as a result of radiative transfer effects (Neufeld 1991; Hansen & Oh 2006; Verhamme, Schaerer & Maselli 2006).

In Figure 3 we show kinematic maps of each of the blobs. At each pixel, we fit a single Gaussian emission line to each SAURON spectrum. We show only those lines which have an amplitude-to-noise¹ $A/N > 3$. The median velocity of the observed field has been subtracted, in order to reveal any velocity shear that may be indicative of outflow or rotation. We also show the velocity dispersion, corrected for the instrumental dispersion. One spatial sampling element is $0.4 \times 0.4 \text{ arcsec}^2$.

Bower et al. (2004) identified a velocity shear in the C15 system, and this is confirmed in the deeper data. The system has a peak to peak shear of $\sim 250 \text{ km s}^{-1}$. The velocity field does not have sufficient spatial resolution to distinguish rotation from outflow (or even inflow). However, the orientation of the shear, perpendicular to the axis of the underlying galaxy, is strongly suggestive of outflows such as those seen in the local starburst galaxy M82 (Shopbell & Bland-Hawthorn 1998; Walter, Weiss & Scoville 2002).

A similar velocity field (but with a substantially higher peak-to-peak shear of 550 km s^{-1}) is revealed for LBG C11, although in this case the optical source has no clearly identified axis which can help distinguish between rotation and outflow (or inflow). Weaker evidence for velocity shear is also apparent in R1 (peak-to-peak velocity shear of $\sim 300 \text{ km s}^{-1}$), while R2 and R3 show no detectable shear. This is also illustrated in Figure 4, where we show fits of the observed velocity field (V_{obs}) with a simple rotation description given by

$$V_{\text{obs}} = V_{\text{rot}} \cos(\phi - \text{PA}). \quad (1)$$

Here V_{rot} is the amplitude of the rotation and PA the kinematic position angle. The azimuthal angle ϕ was defined in

¹ We define amplitude-to-noise as the ratio between the amplitude of the fitted Gaussian emission peak and the noise level of the emission free part of the spectrum.

Field	Single Gaussian			Double Gaussian					Gauss + Absorber				
	z	σ km s ⁻¹	χ^2	z_1	σ_1 km s ⁻¹	z_2	σ_2 km s ⁻¹	χ^2	z_G	σ_G km s ⁻¹	z_A	EW_A km s ⁻¹	χ^2
C15	3.098	280	22	3.098	270	3.089	109	21	3.099	294	3.109	379	22
R1	3.100	356	37	3.096	137	3.103	251	20	3.100	385	3.090	100	29
R2	3.099	409	23	3.093	216	3.101	302	17	3.099	386	3.098	20	18
R3	3.100	464	56	3.092	236	3.102	292	21	3.099	399	3.097	275	22
C11	3.099	476	56	3.101	108	3.098	545	33	3.098	422	3.095	280	38

Table 2. Parameters of the fitted profiles (see Figure 2) to the Ly α emission lines in selected regions in LAB1. For the Gaussian profiles we show redshift z and velocity dispersion σ , and for the Voigt absorber redshift z , and effective width EW . The column density n was fixed to $3 \times 10^{14} \text{ cm}^{-2}$ for each region. The instrumental dispersion ($\sigma = 108 \text{ km s}^{-1}$) has been taken into account.

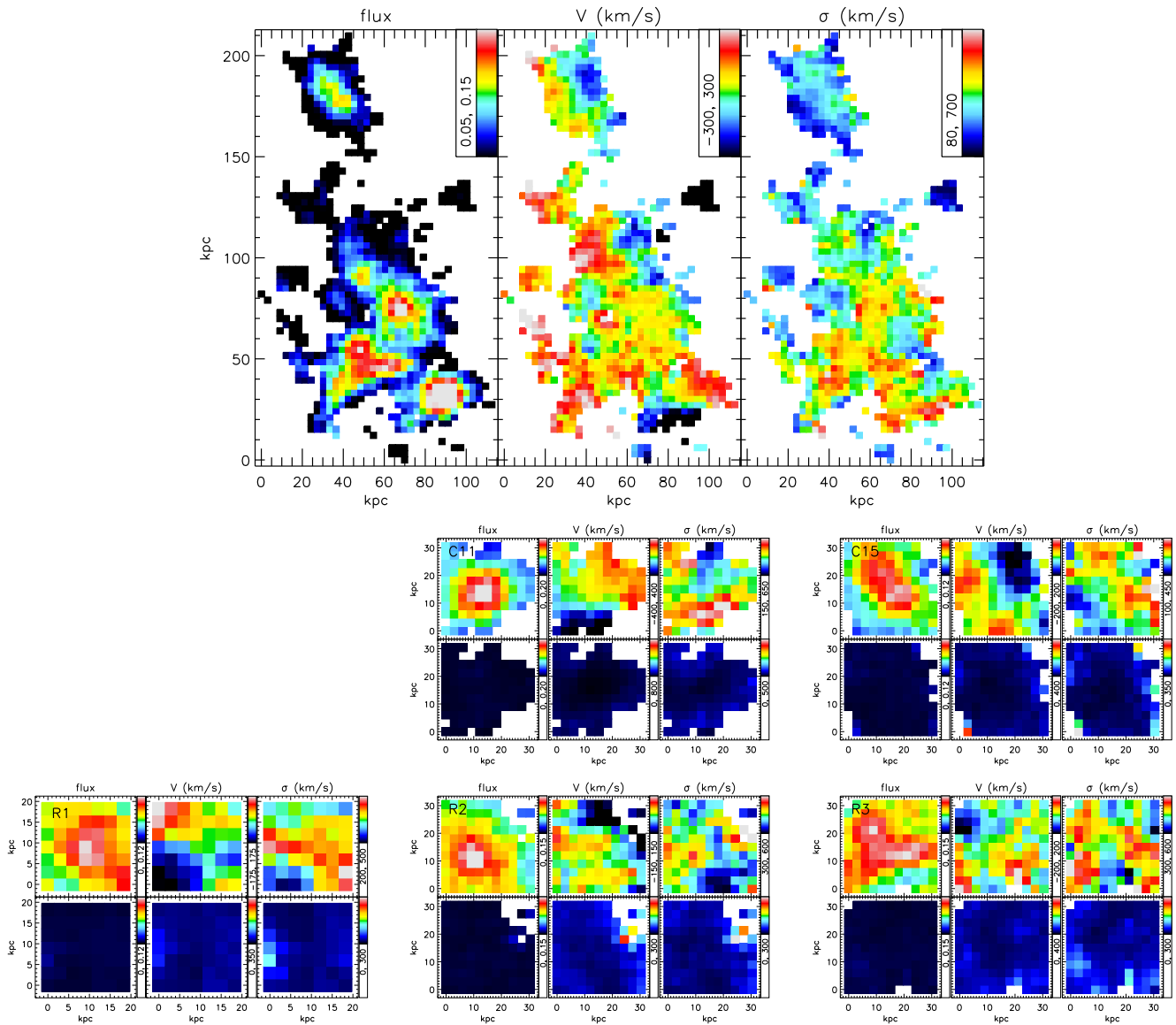


Figure 3. Kinematic maps of the Ly α gas in LAB1. Top figure shows the total LAB1 region, with from left to right: flux (in arbitrary units), velocity (km s⁻¹) and velocity dispersion (km s⁻¹), obtained by fitting a single Gaussian line to each separate SAURON spectrum. The colour scale is indicated in the upper right corner of each plot, and only lines with amplitude-to-noise $A/N > 3$ are shown. In the remaining figures we show blow-ups of C11 and C15 (middle row, from left to right) and R1, R2 and R3 (bottom row, from left to right). Top figures of each panel show the kinematic maps (flux, velocity and velocity dispersion), while the bottom figures show on the same colour scale the corresponding error (1σ) maps, obtained by Monte Carlo simulations.

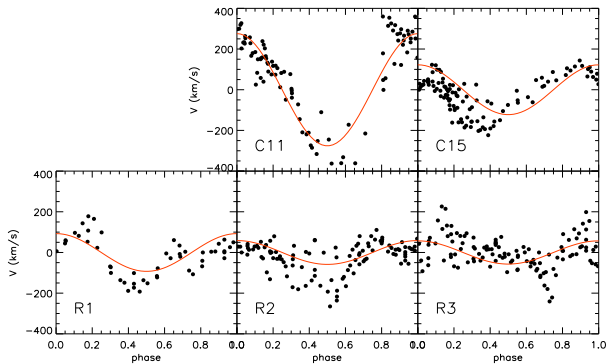


Figure 4. Rotation signatures in the Ly α regions identified in LAB1. With black dots we show the observed velocities, and the red solid line represents the best cosine fit to the data (see text and Equation 1). The regions C11, C15 and R1-R3 are indicated in the lower-left corner for each plot. C11, C15 and possibly R1 show velocity shear signatures, while R2 and R3 do not.

the standard way with respect to a central pixel (x_c, y_c) . For C11 and C15 we were able to fit for this central pixel, but for R1-R3 the fit was noisier, and instead we fixed x_c and y_c to the geometrical centre of the field, which coincides with the peak of the Ly α emission. These fits show more quantitatively than the velocity maps the absence of a shear pattern in R2 and R3, while C11 and C15 (and to a smaller extent also R1) have clear signatures of velocity shears. If rotation were indeed responsible for the observed line widths, then we infer dynamical masses for the separate blobs of 8×10^{11} - $2 \times 10^{12} M_\odot$, in agreement with the findings of Matsuda et al. (2006). If however outflows are the main driver for the line widths, then the corresponding timescales vary between 6×10^7 and 1×10^8 yr, also in agreement with Matsuda et al. (2006).

In Figure 5 we show spectra of individual spatial elements for the central parts of the emission regions C15 and R3. Also indicated for each spectrum is the centre of the single Gaussian fit to the total spectrum of these regions (see Figure 2). The velocity shear in the NE-SW direction is clearly visible in C15. Note however that most of the flux in C15 is aligned perpendicular to this axis, so that the summed spectrum in Figure 2 indeed is well approximated by a single Gaussian line. In R3 the line profiles and flux distribution is however more complex.

Although it is difficult to discern trends on the basis of so few objects (C11 and C15), it seems that outflows are common in the systems where an unobscured galaxy is associated with the source of emission. A much larger sample is needed to draw any quantitative conclusions.

Interestingly, Shapiro et al. (2008) analysed velocity and dispersion maps of starforming galaxies around $z \sim 2$, using the H α emission line. They found that several of their galaxies could be described by rotating discs. Ly α velocity maps are more difficult to interpret, as Ly α is a resonant line and traces the surface of last scattering. While the H α emission line traces the ionised gas in the galaxy disc, Ly α lines can also probe the large-scale diffuse gas structure. Thus it is likely that the two emission lines probe different gas regimes, and are highly complementary for studying the formation of young galaxies.

4 DISCUSSION AND CONCLUSIONS

We have presented very deep integral-field spectrograph observations of the LAB1 Ly α emission halo. The deep data allow us to study the spatial and velocity structure of this system in unprecedented detail.

We find that the giant halo is made up from a superposition of five distinct blobs, with the emission from these regions accounting for at least 55 per cent of the total diffuse flux. Most of the emission regions are associated with individual galaxies. The regions C15 and C11 are associated with optical Lyman Break Galaxies and region R3 is associated with a bright submillimeter source. While this source is faint in the optical, it is bright at $3.6 \mu\text{m}$, suggesting that it is a strongly dust-obscured starforming galaxy. None of these sources are detected at X-ray wavelengths, suggesting that it is unlikely that the emission is powered by an AGN. The regions R1 and R2 are not associated with any optical or IR source, and the emission from these blobs plausibly comes from gas associated with the proto-cluster potential.

The integral-field spectra allow us to examine the emission line profiles and velocity structure in each of the blobs. In R1, R3 and C11, we find that the integrated emission line profiles are not adequately fitted by a single component Gaussian, and that a better fit is obtained with either a two component Gaussian or the combination of a Gaussian emission and Voigt absorption line profile. We find that the underlying emission has a velocity centroid that is extremely similar from region to region, reinforcing the idea that the LAB1 system is a virialised group with velocity dispersion $\sim 100 \text{ km s}^{-1}$. However, in contrast to the LAB2 system, we find no evidence for a coherent shell of absorption that covers the entire system. Any absorption features are significantly weaker than those seen in LAB2, so that they might arise in the large-scale structure foreground to the proto-cluster.

C15, C11 and possibly R1 show evidence of coherent velocity shear arising from an outflow or rotation. In C15 the velocity gradient is perpendicular to the morphology of the underlying galaxy, consistent with the pattern expected for an outflowing galactic wind. In the other systems the relation between the velocity field and the underlying galaxy is unclear. The velocity shear is largest in C11 where it is $\sim 550 \text{ km s}^{-1}$ over approximately 25 kpc. The implied outflow velocity is comparable with that seen in many other Lyman break systems, and does not suggest that the sources seen in LAB1 are undergoing unusually strong feedback.

The primary motivation for these observations was to discover whether the coherent absorption systems such as seen by Wilman et al. (2005) in LAB2 are a ubiquitous feature. These observations have shown that they are not. The data for LAB2 are best interpreted as a large-scale superbubble of material that has been expelled by a high power, perhaps explosive feedback event. The two LAB systems both seem to be made up of smaller emission clouds. So why does the absorption pattern in LAB1 and LAB2 differ? One possible answer is that a similar event has occurred in LAB1 in the past, but that the shell has now broken up, as it passed through the intergalactic medium of this proto-cluster, or that it is sufficiently blue shifted that it cannot be seen in absorption against the system's Ly α emission. Another explanation might be that LAB1 is a younger system in which the large scale outflow is yet to develop. This

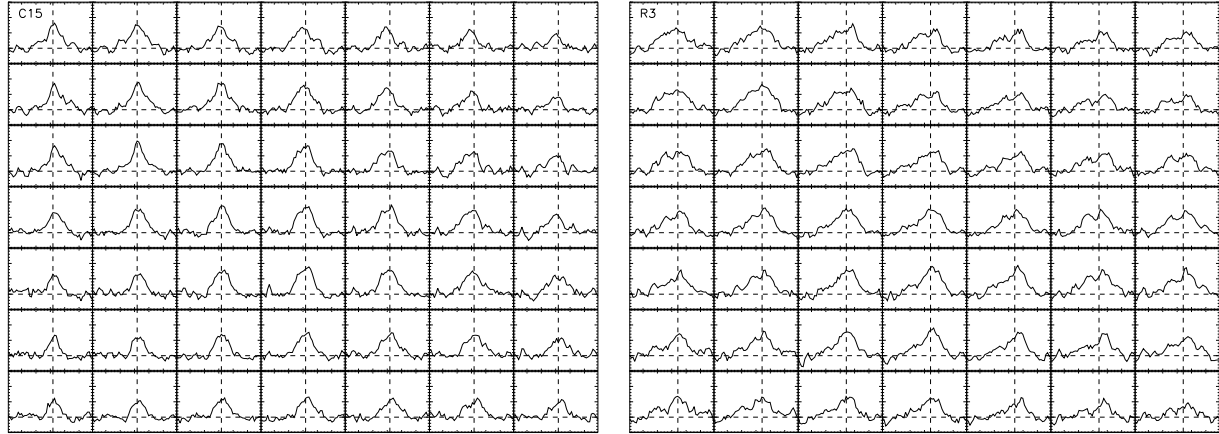


Figure 5. Spectra of individual spatial elements (0.4 arcsec) of the central regions of C15 (left) and R3 (right). We show the central 49 spectra over a wavelength range centred on the Ly α line (4950 to 5010 Å). The vertical line is the same in each panel and denotes the centre of the single Gaussian fit to the summed spectrum in the region (see Figure 2).

seems unlikely, however, since we see no signs of spectacular outflows associated with the individual emission systems. Now that we have dissected the giant emission halo into a number of smaller systems, these seem quite comparable to the many radio quiet LAB systems identified by Matsuda et al. (2004). In many ways, the composite system represents a microcosm of diffuse Ly α emission in general, with the systems reflecting a diversity of power sources. Geach et al. (2009) favour photo-ionisation as the principle power source for LABs. This fits in well with C11, C15 and R3 (if we allow for the possibility that it is only so strongly obscured along our line of sight). However, this appears to describe the R1/R2 emission less well. Possibly the emission from this part of the system is much more closely related to the emission seen around radio galaxies (Chambers et al. 1990; Villar-Martín et al. 2002) and (perhaps) in local cooling flow clusters (Johnstone & Fabian 1988).

ACKNOWLEDGEMENTS

We would like to thank the anonymous referee for comments and suggestions, which helped to improve the presentation of our work. It is a pleasure to thank Michele Cappellari, Eveline van Scherpenzeel, Chris Benn and the ING staff for support on La Palma. We gratefully acknowledge Huub Röttgering, Joop Schaye, Kristen Shapiro and Ian Smail for fruitful discussions, and Roland Bacon and Eric Emsellem for their help in the initial stages of this project.

This research was supported by the Netherlands Research School for Astronomy NOVA, and by the Netherlands Organization of Scientific Research (NWO) through grant 614.000.426. AW acknowledges The Leids Kerkhoven-Bosscha Fonds and the European Southern Observatory for contributing to working visits. AMS and JEG acknowledge support from STFC.

The SAURON observations were obtained at the William Herschel Telescope, operated by the Isaac Newton Group in the Spanish Observatorio del Roque de los Muchachos of the Instituto de Astrofísica de Canarias.

REFERENCES

- Bacon R. et al., 2001, *MNRAS*, 326, 23
 Blain A.W., Barnard V.E., Chapman S.C., 2003, *MNRAS*, 338, 733
 Bower R.G. et al., 2004, *MNRAS*, 351, 63
 Chambers K.C., Miley G.K., van Breugel W.J.M., 1990, *ApJ*, 363, 21
 Chapman S.C., Lewis G.F., Scott D., Richards E., Borys C., Steidel C.C., Adelberger K.L., Shapley A.E., 2001, 548, 17
 Chapman S.C., Scott D., Windhorst R.A., Frayer D.T., Borys C., Lewis G.F., Ivison R.J., 2004, *ApJ*, 606, 85
 de Zeeuw P.T. et al., 2002, *MNRAS*, 329, 513
 Dijkstra M., Haiman Z., Spaans M., *ApJ*, 649, 14
 Dijkstra M., Loeb A., 2009, *MNRAS*, submitted (arXiv0902.2999)
 Fardal M.A., Katz N., Gardner J.P., Hernquist L., Weinberg D.H., Davé R., 2001, *ApJ*, 562, 605
 Ferland G.J., Fabian A.C., Hatch N.A., Johnstone R.M., Porter R.L., van Hoof P.A.M., Williams R.J.R., 2009, *MNRAS*, 392, 1475
 Geach J.E. et al., 2005, *MNRAS*, 363, 1398
 Geach J.E., Smail I., Chapman S.C., Alexander D.M., Blain A.W., Stott J.P., Ivison R.J., 2007, *ApJ*, 655L, 9
 Geach J.E. et al., 2009, *ApJ*, 700, 1
 Haiman Z., Spaans M., Quataert E., 2000, *ApJ*, 537, 5
 Hansen M., Oh S.P., 2006, *MNRAS*, 367, 979
 Heckman T.M., Armus L., Miley G.K., 1990, *ApJS*, 74, 833
 Ivison R.J., et al., 2007, *MNRAS*, 380, 199
 Johnstone R.M., Fabian A.C., 1988, *MNRAS*, 233, 581
 Kennicutt R.C., 1998, *ApJ*, 498, 541
 Kuntschner H., et al., 2006, *MNRAS*, 369, 497
 Matsuda Y., et al., 2004, *AJ*, 128, 569
 Matsuda Y., Yamada T., Hayashino T., Yamauchi R., Nakamura Y., 2006, *ApJ*, 640, L123
 Matsuda Y., Iono D., Ohta K., Yamada T., Kawabe R., Hayashino T., Peck A.B., Petitpas G.R., 2007, *ApJ*, 667, 667
 Neufeld, D.A., 1991, *ApJ*, 370L, 85
 Nilsson K.K., Fynbo J.P.U., Møller P., Sommer-Larsen J., Ledoux C., 2006, *A&A*, 452, 23
 Ohyama Y. et al., 2003, *ApJ*, 591, 9
 Shapiro K.L. et al., 2008, *ApJ*, 682, 231
 Shapley A.E., Steidel C.S., Pettini M., Adelberger K.L., Erb D.K., 2006, *ApJ*, 651, 688
 Shoppell P.L., Bland-Hawthorn J., 1998, *ApJ*, 493, 129
 Smith D.J.B., Jarvis M.J., 2007, *MNRAS*, 378, L49

- Smith D.J.B., Jarvis M.J., Lacy M., Martínez-Sansigre A., 2008, MNRAS, 389, 79
- Steidel C.S., Adelberger K.L., Shapley A.E., Pettini M., Dickinson M., Giavalisco K., 2000, ApJ, 532, 170
- Taniguchi Y., Shioya Y., 2000, ApJ, 532, 13
- Verhamme A., Schaerer D., Maselli A., 2006, A&A, 460, 397
- Villar-Martín M., Vernet J., di Serego Alighieri S., Fosbury R., Pentericci L., Cohen M., Goodrich R., Humphrey A., 2002, MNRAS, 336, 436
- Walter F., Weiss A., Scoville N., 2002, ApJ, 580L, 21
- Wilman R.J., Jarvis M.J., Röttgering H.J.A., Binette L., 2004, MNRAS, 351, 1109
- Wilman R.J., Gerssen J., Bower R.G., Morris S.L., Bacon R., de Zeeuw P.T., Davies R.L., 2005, Nature, 436, 227
- Weijmans A., et al., 2009, MNRAS, 398, 561